



Research paper

Novel β -NiS film modified CdS nanoflowers heterostructure nanocomposite: Extraordinarily highly efficient photocatalysts for hydrogen evolution

Yu Zhang^{a,b,c}, Zhijian Peng^{a,b,*}, Shundong Guan^{b,c}, Xiuli Fu^{c,*}



^a School of Engineering and Technology, China University of Geosciences, Beijing 100083, PR China

^b School of Science, China University of Geosciences, Beijing 100083, PR China

^c State Key Laboratory of Information Photonics and Optical Communications, and School of Science, Beijing University of Posts and Telecommunications, Beijing 100876, PR China

ARTICLE INFO

Keywords:
 NiS/CdS nanoflowers heterostructure
 Water splitting
 Photocatalysts
 Cocatalyst
 Hydrothermal synthesis

ABSTRACT

The compositing of semiconductor based photocatalysts with cocatalysts is a well-known, effective strategy to acquire high hydrogen evolution efficiency, for which their morphology and composition are the concerns of most literatures. However, the contact between them, which has been always difficult to improve, is also a key factor. Here a novel β -NiS film modified CdS nanoflowers (NiS/CdS NFs) heterostructure nanocomposite (HSNC) was successfully synthesized through a simple one-pot hydrothermal method. The obtained NiS/CdS NFs HSNC has well-constructed integrated structure of strong adhesion between the semiconducting CdS NFs and the cocatalyst NiS thin films, displaying good transfer ability to photogenerated electrons and high adsorption to visible light together. Resultantly, the obtained composite presents extraordinarily highly efficient photocatalytic hydrogen evolution, and high chemical and structural stability in aqueous solution containing 20 vol.% lactic acid under visible light. The highest rate for hydrogen production reached a recorded value of about $30.1 \text{ mmol h}^{-1} \text{ g}^{-1}$ at 25°C among all CdS-NiS composite catalysts, and the highest apparent quantum efficiency was approximately 43% at 420 nm. The growth and photocatalysis mechanisms for the NiS/CdS NFs were proposed.

1. Introduction

The depletion of fossil energy and the resultant environmental pollution have attracted lots of world-wide attention to find clean energies to replace the traditional fossil energy. Among all the efforts, hydrogen evolution by water-splitting under sunlight has been given great hopes, because hydrogen energy is pollutant-free and of high energy density, and the solar energy is inexhaustible [1–4]. Since the first work on the hydrogen evolution over TiO_2 photocatalyst by Honda [5], a large amount of semiconductor based photocatalysts have been reported for hydrogen production, including various oxides, sulfides, selenides, and phosphides [6,7]. In particular, metal sulfides, which are regarded as suitable candidates for visible light-driven photocatalysts, have been received much attention on account of their unparalleled electrocatalytic functions for cathodic H_2 evolution during the electrolysis of water [8,9]. Among them, n-type semiconductor CdS, with a narrow band gap of 2.4 eV, is a very attractive candidate for photocatalytic hydrogen evolution due to its high activity under visible light and sufficiently negative flat-band potential for the reduction of H^+ to H_2 [10,11]. However, CdS alone always exhibits low hydrogen

evolution rate due to the rapid recombination of photogenerated carriers [12,13]. So, efficient cocatalysts have to be sought for enhancing the photocatalytic property of CdS, because cocatalysts can effectively promote the separation of photogenerated electrons (e^-) or holes (h^+), which is helpful for the decrease of over-potential in H_2 -production reactions [14–17].

In literature, it was reported that, like precious metal Pt, many transition metals (including Mo, W and Ni) sulfides would be also promising cocatalysts for promoting the photocatalytic hydrogen generation over semiconducting CdS [18–21]. In particular, since Zhang et al. [21] first reported the high efficiency of NiS/CdS composite on visible-driven hydrogen evolution in 2010, various nickel sulfide containing CdS photocatalysts have been investigated to search for the efficient cocatalytic property of nickel sulfide [22–24]. As for the synthesis of nickel sulfide containing CdS heterostructures, Qin et al. [25] first introduced a one-step hydrothermal method, obtaining a catalyst of CdS and NiS_x nanoparticles with a much enhanced efficiency on visible-driven hydrogen evolution, due to the high dispersity of individual nanoparticles and the claimed intimate contact between the two components. However, during hydrothermal synthesis, due to the

* Corresponding authors.

E-mail addresses: pengzhijian@cugb.edu.cn (Z. Peng), xiulifu@bupt.edu.cn (X. Fu).

great lattice mismatch between nickel sulfide and CdS, nickel sulfide is prone to precipitate onto CdS nanostructures in the form of particles, which limits the enhancement on the contact area between them, and thus their performance for photocatalytic hydrogen evolution [18].

On the other hand, sodium hypophosphite monohydrate ($\text{NaH}_2\text{PO}_2\text{H}_2\text{O}$) is a common reducing agent for electroless plating, which can facilitate the deposition of metals, alloys and/or compounds films onto the surface of various target materials with good adhesion [26,27]. In particular, many investigations have been carried out for electroless Ni plating onto different substrates by using $\text{NaH}_2\text{PO}_2\text{H}_2\text{O}$ into electroplating solution, such as carbon fibers, graphene and polyester fabric [28–30], where the deposited Ni films might further react with other chemicals to synthesize Ni-containing compounds. For example, Lee et al. [31] prepared web-like carbon fibers coated with $\text{Ni}_3\text{S}_2/\text{Ni}$ particles by firstly electroless Ni plating onto the pre-woven fibers via using $\text{NaH}_2\text{PO}_2\text{H}_2\text{O}$ and then subsequent sulfuration with S powder in $(\text{NH}_4)_2\text{S}_x$ solution, but the loaded Ni_3S_2 onto the carbon fibers was still of particles. Moreover, to the best of our knowledge, there is no report on the electroless Ni plating on the surface of semiconductors. Thus we wonder if nickel sulfide can be synthesized on the surface of host photocatalysts by electroless Ni plating and corresponding sulfuration, and whether the resultant nickel sulfide can have highly adhesive contact with the host photocatalysts.

Therefore, in this work, we propose a one-pot hydrothermal method for the synthesis of a novel β -NiS film modified CdS nanoflowers (NiS/CdS NFs) heterostructure nanocomposite (HSNC) via electroless Ni plating from the commonly used cadmium, nickel and sulfur sources by employing $\text{NaH}_2\text{PO}_2\text{H}_2\text{O}$ as the reducing agent. The optimally obtained NiS/CdS NFs HSNC shows extraordinarily high efficiency for photocatalytic hydrogen evolution, and chemical and structural stability in aqueous solution containing lactic acid under visible light, reaching a recorded hydrogen production rate of about $30.1 \text{ mmol h}^{-1} \text{ g}^{-1}$ at 25°C among all CdS-NiS composite catalysts, due to the large amount of active sites on the surface of the composite originating from the excellent contact between the highly conductive β -NiS film and excellently visible-light-absorptive CdS NFs.

2. Experimental section

2.1. Raw chemicals

The applied cadmium nitrate tetrahydrate ($\text{Cd}(\text{NO}_3)_2 \cdot 4\text{H}_2\text{O}$, > 98.0%), nickel acetate tetrahydrate ($\text{Ni}(\text{CH}_3\text{COO})_2 \cdot 4\text{H}_2\text{O}$, > 98.0%), sodium hypophosphite monohydrate ($\text{NaH}_2\text{PO}_2\text{H}_2\text{O}$, 98.0 ~ 103.0%), lactic acid ($\text{C}_3\text{H}_6\text{O}_3$, > 85.0%) and sodium sulfite anhydrous (Na_2SO_3 , > 97.0%) were bought from Sinopharm Chemical Reagent (Shanghai, China). Thiourea ($\text{CH}_4\text{N}_2\text{S}$, > 99.0%) and sodium sulfide nonahydrate ($\text{Na}_2\text{S}_2 \cdot 9\text{H}_2\text{O}$, > 98.0%) were commercially available from Xilong Chemical (Shanghai, China). All chemicals were used as received without further purification.

2.2. Samples preparation

2.2.1. NiS/CdS NFs HSNCs

The NiS/CdS NFs HSNCs were synthesized by a one-pot hydrothermal method. After a series of investigations, an optimal NiS/CdS NFs HSNC, which consists of pure β -NiS and CdS and possesses the highest photocatalytic activity under the designed conditions, was synthesized (see details in Table 1 and Figs. 1–10 in Ref. [32]). During the synthesis under the optimized conditions, 1 mmol of $\text{Cd}(\text{NO}_3)_2 \cdot 4\text{H}_2\text{O}$, 3 mmol of $\text{CH}_4\text{N}_2\text{S}$, 0.6 mmol of $\text{Ni}(\text{CH}_3\text{COO})_2 \cdot 4\text{H}_2\text{O}$ and 0.6 mmol of $\text{NaH}_2\text{PO}_2\text{H}_2\text{O}$ were in turn added into 50 mL of deionized water with vigorous magnetic stirring. When it became transparent, the solution was transferred into a Teflon autoclave of 100 mL capacity for hydrothermal treatment at 180°C for 4 h. After cooling down naturally

to room temperature, the obtained dark yellow precipitate was filtered off, washed with distilled water and absolute ethanol for several times, and finally dried in a vacuum oven at 60°C for 12 h.

2.2.2. Pure CdS NFs and NiS nanopowder (NP)

The pure CdS NFs were prepared through using the similar hydrothermal processes and parameters with those for the optimal NiS/CdS NFs HSNC but without $\text{Ni}(\text{CH}_3\text{COO})_2 \cdot 4\text{H}_2\text{O}$ and $\text{NaH}_2\text{PO}_2\text{H}_2\text{O}$. Finally, a reddish orange powder-like solid would be obtained (also see Table 1 in Ref. [32]). And similarly, the pure NiS NP was synthesized through using the similar hydrothermal processes and parameters with those for the optimal NiS/CdS NFs HSNC without $\text{Cd}(\text{NO}_3)_2 \cdot 4\text{H}_2\text{O}$ but in the presence of 0.6 mmol $\text{NaH}_2\text{PO}_2\text{H}_2\text{O}$. At last, a black powder was obtained (also see Table 1 in Ref. [32]).

2.2.3. NiS-CdS mechanical mixing composite (MMC)

The NiS-CdS MMC was prepared by mechanically mixing pure CdS NFs and NiS NP. During the preparation, the applied CdS NFs and NiS NP were firstly synthesized by the above hydrothermal method. Subsequently, with a Ni/Cd molar ratio of 0.6 as the feed molar ratio (FMR) for preparing the optimal NiS/CdS NFs HSNC, they were dispersed into 10 mL absolute ethyl alcohol in an agate mortar. After full mixing by grinding, the suspension was dried in a vacuum oven at 60°C for 12 h. An orange solid was obtained after cooling down to room temperature.

2.3. Materials characterization

The X-ray powder diffraction (XRD) pattern of the as-prepared samples was recorded on a Rigaku D/max-RB X-ray diffractometer equipped with graphite monochromatized $\text{Cu K}\alpha$ radiation ($\lambda = 1.5418 \text{ \AA}$) in a continuous scanning mode at a rate of $6^\circ/\text{min}$. The microstructure of the samples was examined by a field emission scanning electron microscope (FE-SEM, S4800) and transmission electron microscope (TEM, FEI Tecnai G2 F30 U-TWIN). An energy-dispersive X-ray (EDX) spectroscope attached to the TEM was applied to examine their elemental compositions. X-ray photoelectron spectroscopy (XPS, non-monochromated Mg K α radiation, photon energy 1253.6 eV) was conducted to investigate the chemical state and composition of the samples, and the results were calibrated by the binding energy of C 1 s line (284.8 eV). Inductively coupled plasma optical emission spectrometer (ICP-OES, VISTA-MPX) was adopted to measure the content of elements in the samples. The UV-vis absorption spectra were recorded on an UV-vis spectrophotometer (Varian Cary 5000, USA). Photoluminescence (PL) measurements were conducted at room temperature on an IK3202R-D spectrometer by using a He-Cd laser (325 nm) as the excitation source.

2.4. Evaluation of photocatalytic activity

Photocatalytic water splitting reactions were carried out in a Pyrex reaction cell connected to a closed gas circulation and evacuation system (Perfectlight, Beijing, China). The reaction cell was kept at 25°C with cooling water. Typically, 0.02 g of a photocatalyst was dispersed in 100 mL of aqueous solution containing 20 vol.% lactic acid as the sacrificial reagent. The resultant suspension was then thoroughly degassed and irradiated by visible light ($\lambda \geq 420 \text{ nm}$) provided by a 300 W Xe lamp (MICROSOLAR300) equipped with an UV cut-off filter. The amount of hydrogen evolved was determined with an online gas chromatograph (GC-7900, TCD, N_2 carrier gas).

The apparent quantum efficiency (QE%) for the photocatalytic reactions was defined by the following equation,

$$\begin{aligned} \text{QE\%} &= \frac{\text{number of reacted electrons}}{\text{number of incident photons}} \times 100\% \\ &= \frac{\text{number of evolved H}_2\text{molecules} \times 2}{\text{number of incident photons}} \times 100\% \end{aligned} \quad (1)$$

in which, the number of the evolved H₂ molecules was adopted from the amount of H₂ generated during each half hour. And during the test, the light was provided by a 300 W Xe lamp with a band-pass filter ($\lambda = 420 \pm 5$ nm). The average intensity of irradiation was 4.67 mW/cm² measured by a FZ-A irradiatometer (Photoelectric Instrument Factory, Beijing Normal University, Beijing, China), and the irradiation area was 12.57 cm². Thus, the corresponding number of incident photons per second (N) was 1.24×10^{17} (s⁻¹).

2.5. Photoelectrochemical measurements

2.5.1. Working electrode fabrication

Firstly, a sample suspension was prepared by adding 5 mg of the obtained sample into 500 μL of ethanol under consecutively ultrasonic vibration. Then 50 μL of the suspension was dropped onto the surface of a fluorine-doped tin-oxide (FTO) glass substrate (1.5 × 1.5 cm), and dried by nitrogen gas gun at room temperature. After drying, a layer of protective film was coated by dropping 20 μL of Nafion solution (0.5 wt.%) onto the surface of the sample on the FTO glass, finally obtaining a working electrode.

2.5.2. Transient photocurrent tests

Transient photocurrent measurements were performed on a CHI660E electrochemical work station (Chenhua Instrument, Shanghai, China) in a standard three-electrode system with the as-prepared FTO electrodes as the working electrode, a Pt plate as the counter electrode, and Ag/AgCl (saturated KCl) as the reference electrode. An aqueous solution containing 0.1 M Na₂S and 0.02 M Na₂SO₃ was used as the electrolyte. The light was provided by a 300 W Xe lamp with an UV cut-off filter ($\lambda \geq 420$ nm). For the photoresponsive signals, the samples were measured under chopped light at 0 V vs. Ag/AgCl.

2.5.3. Electrochemical impedance spectroscopy (EIS) measurement

The EIS data were collected by the CHI660E electrochemical work station with the above prepared working electrodes in the same three-electrode system under the similar conditions as applied in transient photocurrent tests. The applied frequency was in the range of 0.01–10⁵ Hz, and the AC amplitude was set at 5 mV vs. Ag/AgCl. But all the experiments were conducted in the dark.

3. Results and discussion

3.1. Composition, morphology and microstructure

After a series of investigations, the optimal NiS/CdS NFs HSNC of pure β-NiS and CdS was obtained (also see details in Table 1 and Figs. 1–10 in Ref. [32]). Fig. 1a shows the XRD pattern of the optimal sample together with its optical image. For comparison, those of pure NiS NP, CdS NFs and NiS-CdS MMC are also presented. From Fig. 1a, it can be seen that all the XRD patterns show sharp diffraction peaks, indicating the high crystallinity of them. In the XRD pattern of pure CdS NFs, all the peaks could be indexed to those of hexagonal CdS phase (JCPDS card no. 80-0006), which is often of reddish orange color as shown by this figure. In that of pure NiS NP, all the diffraction peaks of the NiS phase were ascribed to those of the rhombohedral β-NiS phase (JCPDS card no. 86–2280), which is usually a dark solid. In that of the CdS-NiS MMC, both hexagonal CdS and rhombohedral β-NiS phases can be identified. Because it is a mechanically mixing stuff, it presents mixing, orange color from the original CdS NFs and NiS NP. Under the optimized synthesis conditions (also see Fig. 1 in Ref. [32]), the obtained dark yellow NiS/CdS NFs HSNC presents a XRD pattern almost similar with that of the CdS-NiS MMC, from which the characteristic diffraction peaks of hexagonal CdS and rhombohedral β-NiS phases could be identified, revealing that β-NiS co-exists with CdS NFs in the composite.

To detect the adhesion state between CdS and NiS in the NiS/CdS

NFs HSNCs, SEM examination was first carried out, which revealed that under the designed synthesis conditions, the existence of NiS almost had no influence on the morphology of CdS NFs (see Figs. 2 and 7 in Ref. [32]). Typical SEM images on the morphology of the optimal NiS/CdS NFs HSNC are displayed in Fig. 1b and c. The low-magnification SEM image as shown in Fig. 1b reveals that the optimal NiS/CdS NFs HSNC is composed of a large quantity of NFs with an average diameter of 1–4 μm, and each NF consists of many nanodendrites. From the high-magnification SEM image (Fig. 1c), it can be seen that the nanodendrites are composed of a large quantity of irregular aggregated nanoparticles with an average diameter of about 60 nm. Typical EDX spectrum on one whole SEM image (see Fig. 1d) indicates the existence of Ni, Cd, and S elements in the product, which is further confirmed by the local elemental mapping results on the optimal NiS/CdS NFs HSNC (see Fig. 1e–i), revealing that NiS nanocrystals are successfully loaded onto the surface of CdS nanocrystals. Moreover, Ni and S signals could be detected all over the scanning area in the elemental mapping image (see Fig. 1f–h), indicating that the NiS nanocrystals are homogenously distributed over the CdS nanocrystals. Considering the facts that pure β-NiS has a nanoplate-like morphology (see Fig. 3 in Ref. [32]) and the loading of NiS has no obvious effect on the morphology of CdS NFs (see Figs. 2 and 7 in Ref. [32]), it can be deduced that the NiS nanocrystals were coated onto the surface of CdS NFs, i.e., they should behave like a film on the surface of CdS NFs. And this result was further confirmed by the low-magnification TEM image as shown in Fig. 1j, where no NiS nanocrystals could be observed on the surface of CdS NFs. However, the HRTEM image on the optimal NiS/CdS NFs HSNC (see Fig. 1k) reveals that two sets of crystalline lattices could be identified in the composite. The lattice spacing of 0.27 nm could be assigned to the (300) plane of rhombohedral β-NiS, while the one of 0.33 nm could be attributed to the (002) plane of hexagonal CdS. These results are completely consistent with their XRD patterns presented above. And more interestingly, the NiS crystalline lattices could be observed all over the composite together with the CdS crystalline lattices, indicating that the NiS nanocrystals behave as a film, which is in accordance with the results of elemental mapping analysis (Fig. 1e–j), and implying that there exists an intimate contact between the NiS and CdS nanocrystals due to the atomic level bonding between them (also Fig. 4 in Ref. [32]). In addition, according to Fig. 5 in Ref. [32], from the lattice fringe of pure CdS NFs, only (002) plane of hexagonal CdS can be identified, which is completely different from that of Fig. 1k, further confirming the results of Fig. 1e–j. Based on the above results, it is believable that a β-NiS film was successfully coated on the CdS NFs with highly adhesive contact between them.

To analyze the chemical state of the elements in the optimal NiS/CdS NFs HSNC, XPS measurement was further carried out. Fig. 2a is a typical survey spectrum of the sample, which indicates the presence of Cd, Ni, and S in it. Moreover, from the high-resolution XPS results, it can be seen that, the peaks of S 2p at 161 and 162.4 eV (see Fig. 2b) are consistent with the reported values of S 2p_{3/2} and S 2p_{1/2} signals for sulfide, respectively [33]; the binding energy values at 405.3 and 412 eV of Cd 3d (See Fig. 2c) match well with the reported values of Cd 3d_{5/2} and 3d_{3/2} peaks, respectively [24]; and the satellite peaks centered at 404 and 410.7 eV (see Fig. 2c) may be caused by the incorporation of NiS lattices with CdS ones. The binding energies of Ni 2p_{3/2} were located at 853.7 and 857 eV, presenting a little offset of +1 eV compared with the previously reported value of Ni 2p_{3/2} for NiS, which should be caused by the incorporation of NiS lattices with CdS ones [25]. These results are consistent with XRD and SEM data presented above. Besides, on the recorded XPS spectrum, the calculated Ni/Cd molar ratio for this sample is roughly 1:2.3, which is a little lower than that of their FMR (0.6). In order to further elucidate their distribution, ICP elemental analysis was also performed. The measured Ni/Cd molar ratio in the binary NiS/CdS NFs HSNC is around 1:3.0, which is lower than that of the XPS elemental analysis, indicating that the β-NiS phase exists more on the surface of the CdS NFs, indirectly

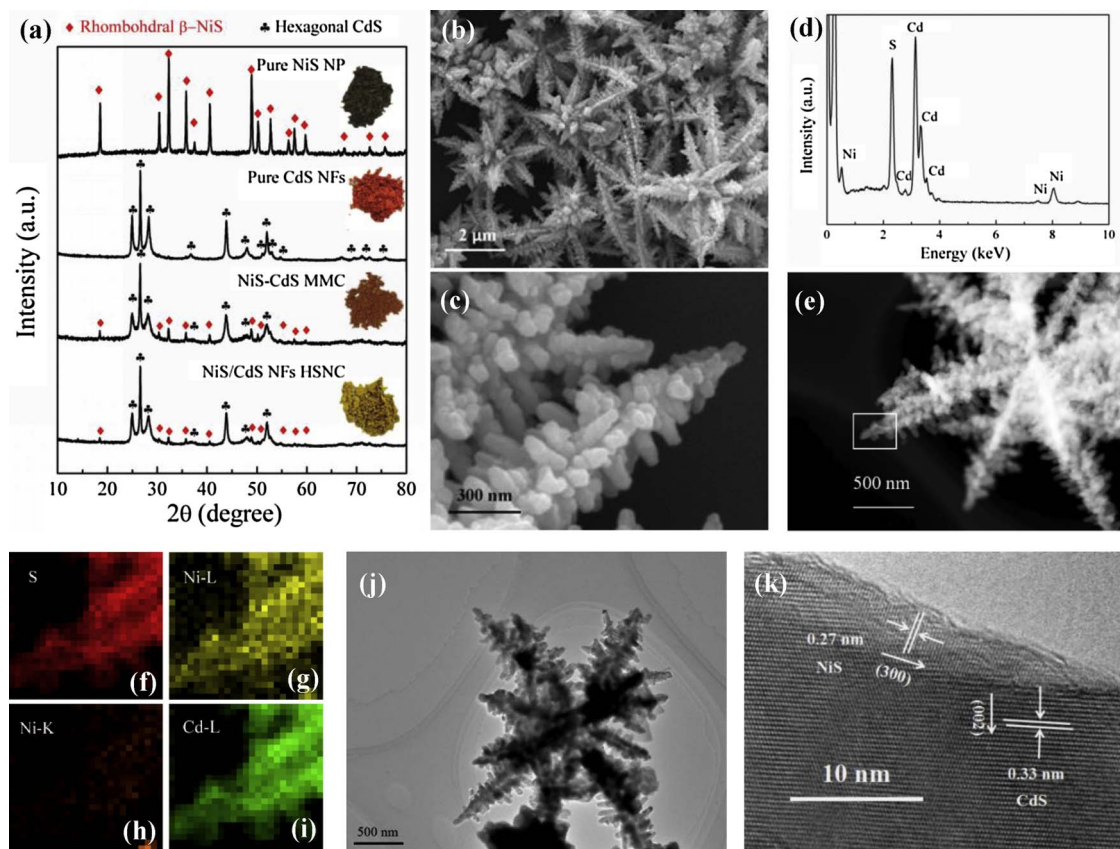


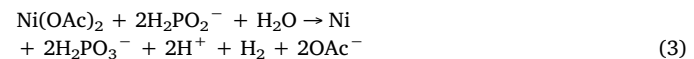
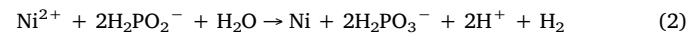
Fig 1. Characterization of the as-synthesized, optimal NiS/CdS NFs HSNC. (a) XRD pattern of the optimal NiS/CdS NFs HSNC in comparison with those of pure NiS NP, CdS NFs and NiS-CdS MMC, where the insets show their optical images. (b) Low-magnification SEM image; (c) high-magnification SEM image and (d) SEM-EDX spectrum of the optimal NiS/CdS NFs HSNC. (e–i) TEM-EDX mapping results of the optimal NiS/CdS NFs HSNC. (j) Low-magnification TEM image and (k) HRTEM image of the optimal NiS/CdS NFs HSNC.

proving that the β -NiS phase is coated on the surface of CdS NFs, behaving like a film.

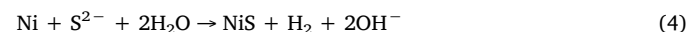
To explore the formation mechanism for the present NiS/CdS NFs HSNCs, the effect of the addition of $\text{NaH}_2\text{PO}_2\cdot\text{H}_2\text{O}$ on the synthesis of NiS/CdS NFs was investigated by controlled experiments, and the results are presented in Table 1 and Figs. 6–10 in Ref. [32]. Under the designed conditions with 1 mmol $\text{Cd}(\text{NO}_3)_2\cdot 4\text{H}_2\text{O}$ and 3 mmol $\text{CH}_4\text{N}_2\text{S}$ (see Table 1a in Ref. [32]), CdS NFs could be directly synthesized due to the strong coordinating ability of $\text{CH}_4\text{N}_2\text{S}$ [34]. When additional 0.6 mmol $\text{Ni}(\text{CH}_3\text{COO})_2\cdot 4\text{H}_2\text{O}$ joined into the reaction system (see Table 1b in Ref. [32]), a precipitate of CdS NFs almost without NiS was obtained, because in this case the added amount of $\text{Ni}(\text{CH}_3\text{COO})_2\cdot 4\text{H}_2\text{O}$ is too less to form a NiS precipitate, which can be confirmed by the test listed in Table 1c in Ref. [32]. By comparing Table 1b and c in Ref. [32], it is seen that in absence of $\text{Cd}(\text{NO}_3)_2\cdot 4\text{H}_2\text{O}$, no precipitate can be obtained just with the same amount of $\text{Ni}(\text{CH}_3\text{COO})_2\cdot 4\text{H}_2\text{O}$ and $\text{CH}_4\text{N}_2\text{S}$. However, also without applying $\text{Cd}(\text{NO}_3)_2\cdot 4\text{H}_2\text{O}$ but via doubling the concentrations of $\text{Ni}(\text{CH}_3\text{COO})_2\cdot 4\text{H}_2\text{O}$ and $\text{CH}_4\text{N}_2\text{S}$ in the reaction system (see Table 1d in Ref. [32]), a composite of cubic Ni_3S_4 , rhombohedral β -NiS and hexagonal α -NiS would be obtained. On the other hand, when a little amount $\text{NaH}_2\text{PO}_2\cdot\text{H}_2\text{O}$ (here 0.6 mmol) was applied in the reaction system, as is seen in Table 1e in Ref. [32], pure β -NiS could be synthesized with as small amount of $\text{Ni}(\text{CH}_3\text{COO})_2\cdot 4\text{H}_2\text{O}$ and $\text{CH}_4\text{N}_2\text{S}$ as in the test of Table 1c in Ref. [32]. SEM imaging revealed that the pure NiS consisted of a large amount of irregular nanoplates aggregating together (see Fig. 3 in Ref. [32]). However, with excessive $\text{Ni}(\text{CH}_3\text{COO})_2\cdot 4\text{H}_2\text{O}$, an impurity phase, $\text{Ni}_{11}(\text{HPO}_3)_8(\text{OH})_6$, would appear in the product together CdS NFs and β -NiS even if $\text{NaH}_2\text{PO}_2\cdot\text{H}_2\text{O}$ was used (as seen in Table 1f in Ref. [32]). Therefore, considering all the above facts, a composite of pure β -NiS film modified pure CdS nanoflowers (the as-reported optimal NiS/CdS NFs) should be

synthesized under the optimized conditions with 1 mmol $\text{Cd}(\text{NO}_3)_2\cdot 4\text{H}_2\text{O}$, 3 mmol $\text{CH}_4\text{N}_2\text{S}$, 0.6 mmol $\text{Ni}(\text{CH}_3\text{COO})_2\cdot 4\text{H}_2\text{O}$ and 0.6 mmol $\text{NaH}_2\text{PO}_2\cdot\text{H}_2\text{O}$ (see Table 1g in Ref. [32]). In a word, an appropriate amount of $\text{NaH}_2\text{PO}_2\cdot\text{H}_2\text{O}$ could promote the synthesis of β -NiS and strengthen the contact of the formed β -NiS film with CdS NFs, which was proceeded through a process based on the electroless Ni plating with $\text{NaH}_2\text{PO}_2\cdot\text{H}_2\text{O}$ as the reducing agent.

In Ref. [35], it was reported that in such reaction, nickel can be electroplated on the surface of an appropriate substrate (here the CdS NFs) at the presence of $\text{NaH}_2\text{PO}_2\cdot\text{H}_2\text{O}$ through the following reactions:



where, the electroplated nickel may distribute homogeneously on the surface of CdS NFs in a form of thin film. After that, the formed nickel film would be sulfurated immediately by S^{2-} from thiourea into NiS through the follow equation owing to the applied high temperature and high pressure:



On the basis of the above results and discussion, a possible formation process for the present NiS/CdS NFs HSNC can be proposed in Fig. 3. Firstly, Cd^{2+} and S^{2-} from thiourea would react to generate CdS seeds, and the CdS seeds will aggregate into the inchoate state of the CdS NFs due to the strong coordinating ability of thiourea [34]. The active Cd^{2+} and S^{2-} would further react to form CdS NFs owing to the preferential growth of the CdS grains. Next, the presence of $\text{NaH}_2\text{PO}_2\cdot\text{H}_2\text{O}$ would promote the loading of Ni thin films onto the surface of the formed CdS NFs through Eqs. (2) and (3), and the newly

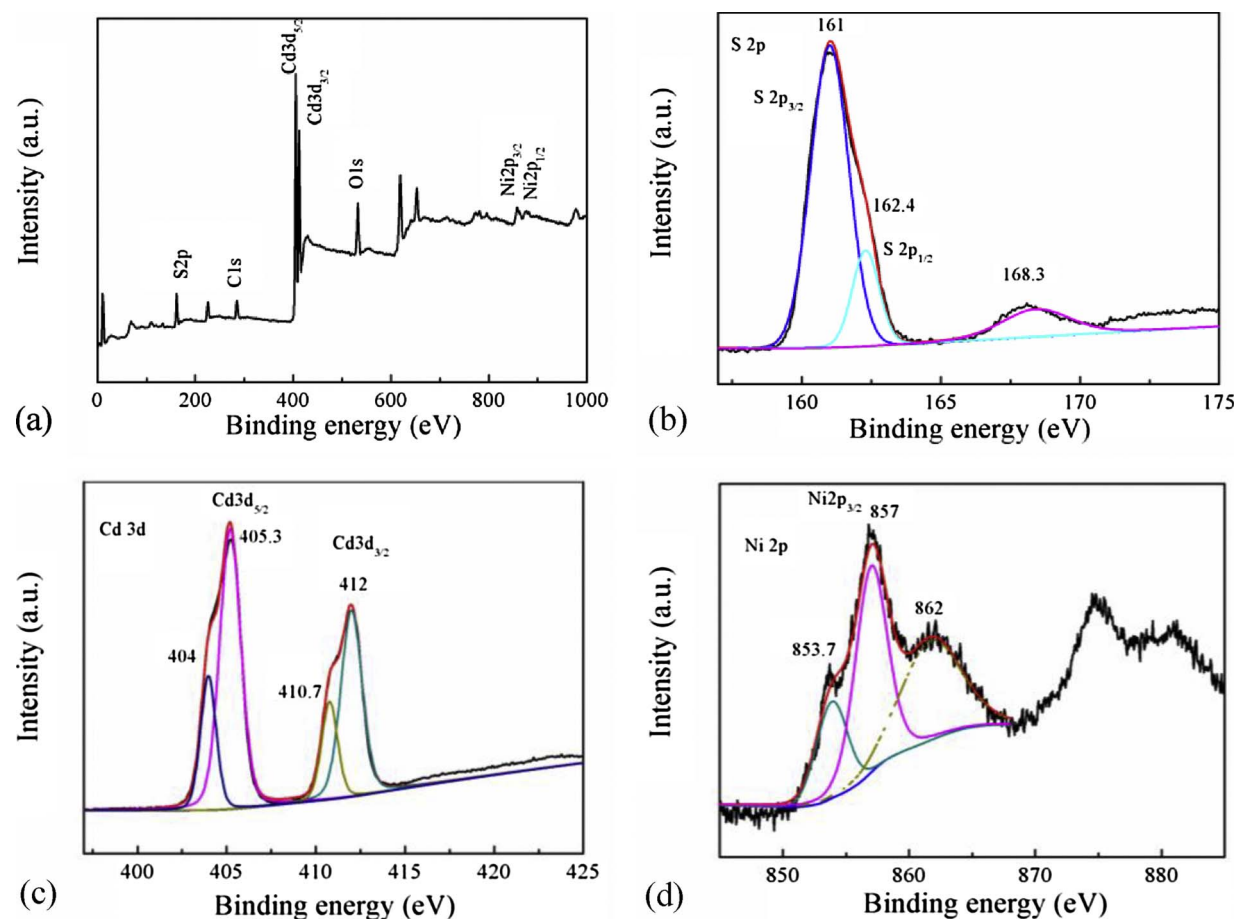


Fig. 2. XPS data of the optimal NiS/CdS NFs HSNC: (a) XPS survey spectrum, and high-resolution XPS spectra of S 2p (b), Cd 3d (c), and Ni 2p (d).

formed Ni film was active, which would react with the active S^{2-} to form a NiS thin film covering on the surface of CdS NFs. With the reaction continuously proceeded, CdS NFs were fully covered by the NiS nanocrystalline film uniformly, forming the final NiS/CdS NFs HSNC. At this stage, a dark yellow NiS/CdS NFs HSNC, which was composed of yellow CdS NFs covered with dark NiS nanocrystalline film, could be collected.

3.2. Photocatalytic activity for hydrogen evolution

Through a series of investigations on the photocatalytic reactions over the obtained samples (see Figs. 11–13 in Ref. [32]), the photocatalytic reaction conditions for the optimal samples were optimized as follows: 20 mg of the photocatalysts was dispersed in a 100 mL of aqueous solution containing 20 vol.% lactic acid; the light was provided by a 300 W Xe lamp with an UV cut-off filter ($\lambda \geq 420$ nm); and the reaction cell was kept at 25 °C by cooling water.

Under the optimized photocatalytic reaction conditions, the

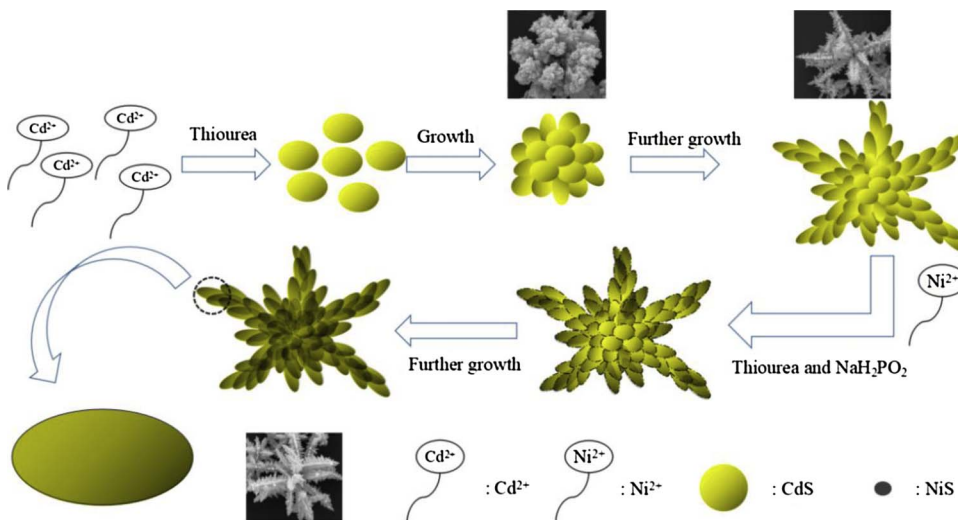


Fig. 3. Schematic of the formation process of the present NiS/CdS NFs HSNC.

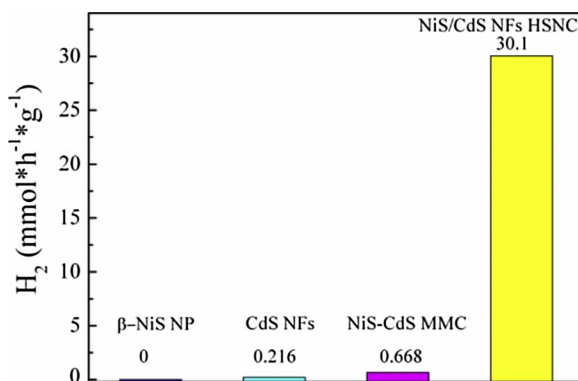


Fig. 4. Photocatalytic activity of the optimal NiS/CdS NFs HSNC under the optimized photocatalytic reaction conditions. For comparison, those of pure NiS NP, CdS NFs and NiS-Cd MMC are also presented.

hydrogen evolution rate (HER) over the optimal NiS/CdS NFs HSNC photocatalyst was obtained; and the result is displayed in Fig. 4. For comparison, those of pure NiS NP, CdS NFs and NiS-Cd MMC are also presented. It can be seen from this figure that pure NiS NP exhibits no photocatalytic activity for hydrogen evolution, revealing that in the present NiS/CdS NFs HSNC photocatalyst, NiS can only act as a cocatalyst. And the HER of pure CdS NFs was rather low

(0.216 mmol $h^{-1} g^{-1}$), while over the NiS/CdS NFs HSNC photocatalyst, the HER increased dramatically, presenting a HER of 30.1 mmol $h^{-1} g^{-1}$, which is about 139 times higher than that of CdS NFs alone and much higher than those over all the CdS-NiS composite catalysts in literatures (see Table 2 in Ref. [32]). This fact indicates that the loading of β -NiS film onto the CdS NFs plays an important role in the enhancement of photocatalytic activity of CdS NFs, clearly revealing that β -NiS is a good cocatalyst for CdS nanostructures during the photocatalytic hydrogen evolution.

In particular, because the loading of NiS onto CdS has no effect on the morphology of the present NiS/CdS NFs HSNC (see Figs. 2 and 7 in Ref. [32]), so the dominant enhancement effects on HER should originate from the cocatalyst effect of NiS for CdS (see Figs. 11 and 12 in Ref. [32]). As for the intrinsic factors that influence the photocatalytic activity of the NiS/CdS NFs HSNCs, one may first check the contribution of the loading amount of NiS. From Figs. 11 and 12 in Ref. [32], it can be seen that for the NiS/CdS NFs HSNC photocatalysts prepared with different Ni/Cd FMRs, the HER increased first and then declined with increasing Ni/Cd FMR or amount of $Na_2PO_2H_2O$, and the highest photocatalytic activity was observed for the NiS/CdS NFs HSNC photocatalyst prepared with a Ni/Cd FMR of 0.6 and 0.6 mmol $Na_2PO_2H_2O$ while the amount of $Cd(NO_3)_2 \cdot 4H_2O$ was fixed at 1 mmol. The increase of HER with the increase of Ni/Cd FMR could be attributed to synergistic effect of the increasing amount of β -NiS film cocatalyst on the CdS NFs, which has high electrical conductivity,

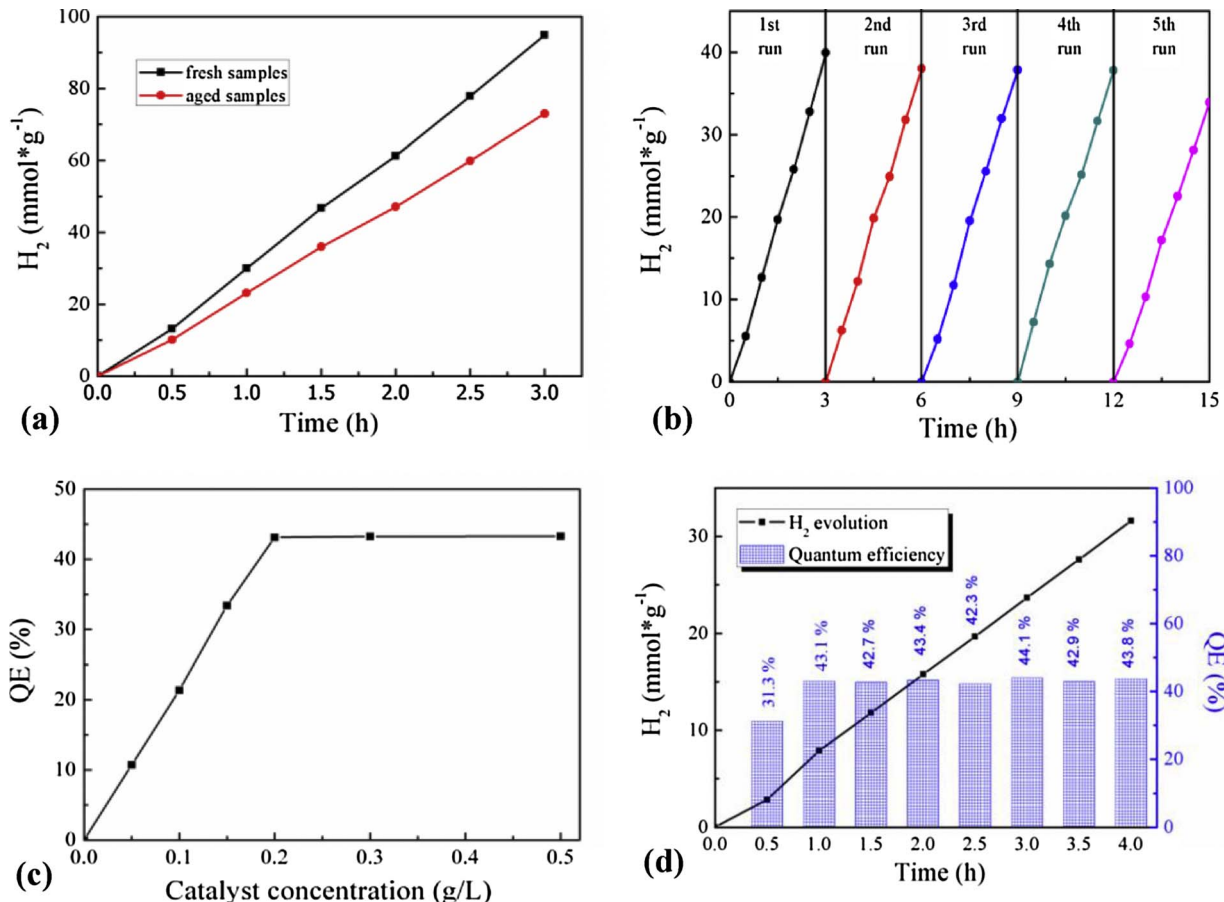


Fig. 5. Photocatalytic hydrogen evolution performance of the optimal NiS/CdS NFs HSNC. (a) The HER under light irradiation ($\lambda \geq 420$ nm) provided by a 300 W Xe lamp with an UV cut-off filter over the fresh NiS/CdS NFs HSNC and its corresponding aged counterpart preserved in a dry and cool condition in air for 4 months. (b) Cycling runs for photocatalytic hydrogen evolution over the optimal NiS/CdS NFs HSNC photocatalyst under the same light irradiation condition as that in (a). During the experiment, after every 3 h, the produced H_2 was evacuated. (c) QE for hydrogen evolution over different catalyst concentrations ($M_{\text{catalyst}}/V_{\text{solution}}$, g/L) in 100 mL of aqueous solution containing 20 vol.% lactic acid over the optimal NiS/CdS NFs HSNC photocatalyst under monochromatic light ($\lambda = 420 \pm 5$ nm) provided by a 300 W Xe lamp with a 420 nm band-pass filter. (d) Hydrogen evolution and QE over the optimal NiS/CdS NFs HSNC photocatalyst with time, in which the experiments were carried out under the same light irradiation condition as that in (c). During the photocatalytic reaction, 20 mg of the optimal NiS/CdS NFs photocatalyst was dispersed in a 100 mL of aqueous solution containing 20 vol.% lactic acid; and the reaction cell was kept at 25 °C by cooling water.

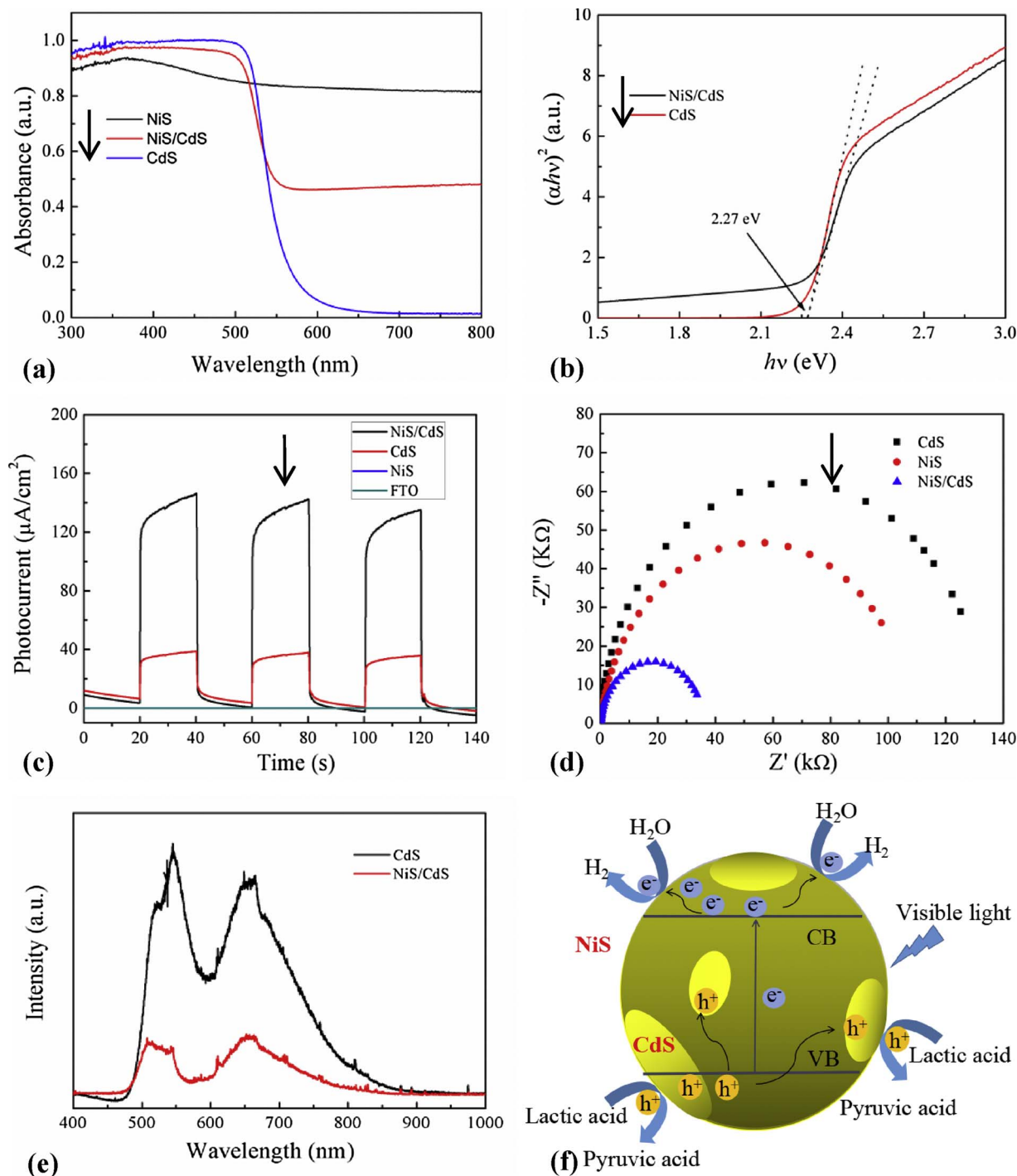


Fig. 6. (a) UV-vis absorption spectra of the pure NiS NP, optimal NiS/CdS NFs HSNC and pure CdS NFs; (b) the curve of $(\alpha h\nu)^2$ versus $h\nu$ for the optimal NiS/CdS NFs HSNC and pure CdS NFs. (c) Transient photocurrent responses of blank FTO, CdS NFs, NiS NP and the optimal NiS/CdS NFs HSNC. (d) EIS Nyquist plots of CdS NFs, NiS NP and the optimal NiS/CdS NFs HSNC. (e) PL spectra of the obtained CdS NFs and NiS/CdS NFs HSNC. (f) Schematic of the photocatalysis mechanism for hydrogen evolution over the present NiS/CdS NFs HSNC under visible light irradiation.

facilitating the transfer of photogenerated electrons during the reaction. The decrease of HER with a higher Ni/Cd FMR or more $\text{NaH}_2\text{PO}_2\text{-H}_2\text{O}$ could be mainly ascribed to the shielding effect of excessive NiS film cocatalyst on CdS NFs [25,36], hindering the absorption to light by the CdS NFs. And the existence of $\text{Ni}_{11}(\text{HPO}_3)_8(\text{OH})_6$ in the samples (see Fig. 1 in Ref. [32]) may be also responsible for the decrease of photocatalytic performance of the samples. Therefore, an appropriate loading amount of NiS is very important for the HER enhancement of CdS. Besides, as is seen from Fig. 4, the HER over the NiS-CdS MMC ($0.668 \text{ mmol h}^{-1} \text{ g}^{-1}$) is apparently higher than that over pure CdS

NFs but much lower than that over the optimal NiS/CdS NFs HSNC photocatalyst, which further confirms the cocatalyst effect of NiS for CdS. And this fact also reveals a stronger contact between the β -NiS film and CdS NFs in the optimal NiS/CdS NFs HSNC than that in the NiS-CdS MMC, which is consistent with discussion in last section (see Fig. 1 in this paper, and Figs. 4 and 5 in Ref. [32]). All these facts further confirm that the applying of $\text{NaH}_2\text{PO}_2\text{-H}_2\text{O}$ could play a crucial role to obtained the present high-performance NiS/CdS NFs HSNC as discussed in last section (also see Table 1 and Figs. 1–10 in Ref. [32]).

As is well known, the stability of a catalyst is very important to its

practical application. Fig. 5a shows the photocatalytic HER over the fresh NiS/CdS NFs HSNC in comparison with that over its corresponding aged counterpart preserved in a dry and cool condition in air for 4 months. As is seen from this figure, after aging 4 months, the photocatalytic HER of the optimal NiS/CdS NFs HSNC decreased to about 77% ($23.1 \text{ mmol h}^{-1} \text{ g}^{-1}$) of that over its fresh counterpart ($30.1 \text{ mmol h}^{-1} \text{ g}^{-1}$), possibly owing to the decomposition of NiS by moisture from the air [21], which would finally decrease the transfer efficiency of the photogenerated electrons. Therefore, as a photocatalyst for H₂ evolution, the as-prepared NiS/CdS NFs HSNC should be kept from air for long-term storage. Moreover, experiments were performed to investigate the photocatalytic stability of the optimal NiS/CdS NFs HSNC for repeating use under visible light irradiation. The reaction system was evacuated every 3 h and the test was repeated for 5 cycles. As is seen from Fig. 5b, there was only very little decrease ($\leq 10\%$) in HER after the fifth cycle. And the decrease of HER should be mainly attributed to the consumption of lactic acid ([37], and also see Fig. 14 in Ref. [32]), although the decomposition of the NiS/CdS NFs HSNC photocatalyst by lactic acid might also play a role [21]. In addition, after cycling tests, XRD and SEM analyses (see Figs. 15 and 16 in Ref. [32]) revealed that almost no changes could be observed in the phase composition and microstructure of the photocatalyst, indicating that the NiS/CdS NFs HSNC is very stable under the designed reaction conditions, because the β -NiS thin films have protection effects for the CdS NFs from the commonly observed photocorrosion on many CdS photocatalysts [38], and the photogenerated holes would prefer to reacting with lactic acid molecules instead of CdS [21]. In a word, the optimal NiS/CdS NFs HSNC photocatalyst could maintain very stable visible-driven photocatalytic activity for H₂ evolution during cycling use.

The QE for H₂ evolution was determined for the photocatalytic systems containing different amounts of the optimal NiS/CdS NFs HSNC catalyst in 100 mL of aqueous solution with 20 vol.% lactic acid under the irradiation of a monochromatic light ($420 \pm 5 \text{ nm}$). The result is illustrated in Fig. 5c. As can be seen from this figure, the QE presents a linear increase with the increase of the adding amount of the photocatalyst in the reaction system, when the applying amount is small. The highest QE (43.1%) was reached in this study when 0.2 g/L or higher concentration of photocatalyst in the reaction system was used, indicating that an appropriate increase in the applied amount of the catalyst is beneficial for the hydrogen evolution due to the enhancement of capturing ability for light. But the additional increase of the photocatalyst cannot further increase the light absorbance, because the incident light was fully applied. Thus, the QE remains unchanged with higher concentration of photocatalyst in the reaction system.

Fig. 5d shows the hydrogen evolution and QE over the optimal NiS/CdS NFs HSNC photocatalyst as a function of time with the optimum concentration (0.2 g/L) of the photocatalyst. The HER reached $7.89 \text{ mmol h}^{-1} \text{ g}^{-1}$ with a QE of about 43.1% after 1 h of reaction. It has to be noted that the apparent HER was lower (roughly $5.87 \text{ mmol h}^{-1} \text{ g}^{-1}$) with a lower QE of about 31.3% in the first 0.5 h of reaction, which may be due to the dissolution of H₂ in the solution during the induction period at the early stage [39]. The QE fluctuates in a very little range during the later reaction, reaching about 42.3%–44.1%, which is a quite high value among those of all the composite catalysts with similar composition (see Table 2 in Ref. [32]). Such highly efficient conversion of visible light energy presumably suggests that the present NiS/CdS NFs HSNC catalyst is highly active for the generation and separation of electron-hole pairs during light irradiation.

In order to elucidate the mechanism of the extraordinarily highly photocatalytic activity for hydrogen evolution over the present NiS/CdS NFs HSNC, its UV-vis absorption spectrum is displayed in Fig. 6a, in comparison with those of the pure NiS NP and CdS NFs. The UV-vis spectrum of the optimal NiS/CdS NFs HSNC displays a significant enhancement in the absorption for the light of a wavelength longer than

520 nm, compared with that of CdS NFs, which can be assigned to the additional absorption of nanocrystalline β -NiS films on the CdS NFs. The band gaps of the obtained CdS NFs and the optimal NiS/CdS NFs HSNC were calculated from the UV-vis diffuse reflectance spectra (see Fig. 6b), which are almost of the same value of 2.27 eV, implying that the β -NiS film was tightly adhesive to the surface of the CdS NFs instead of being doped into the CdS lattice.

To further demonstrate that β -NiS is a good cocatalyst for CdS, the photoelectrochemical properties of the samples were investigated. Fig. 6c shows the photocurrent responses of blank FTO, CdS NFs, NiS NP and the optimal NiS/CdS NFs HSNC under intermittent illumination of visible light. It is easy to find that the photocurrent intensity of NiS NP is equal to that of blank FTO, indicating that there is no photocurrent response for NiS NP sample under visible light. However, the photocurrent intensity of the optimal NiS/CdS NFs HSNC is about 4 times higher than that of pure CdS NFs, implying that the deposition of β -NiS film onto the CdS NFs was beneficial for the separation of photogenerated charges by transporting electrons. In addition, the semi-circles of the EIS spectra (Fig. 6d) are in the sequence of the optimal NiS/CdS NFs HSNC < pure NiS NP < pure CdS NFs, indicating a decrease in the resistance for the charge transfer through the interface layer in the present NiS/CdS NFs HSNC sample. This result confirmed again the effect of β -NiS film on accepting and transporting the photogenerated electrons from the CdS NFs. To further confirm it, PL spectra of the obtained pure CdS NFs and the optimal NiS/CdS NFs HSNC were recorded (see Fig. 6e), which can reflect the transfer efficiency of photogenerated charges [39]. The two emissions of the CdS (at roughly 502 nm) and the defects in CdS (at about 650 nm) were remarkably quenched after the loading of NiS film, which can be attributed to the fast transfer of electrons from CdS NFs to NiS film, thus suppressing the electron-hole recombination and enhancing the photocatalytic activity.

According to the discussion above, a possible mechanism for the photocatalytic hydrogen evolution over the present NiS/CdS NFs HSNC is schematically proposed in Fig. 6f. During visible light irradiation, electron-hole ($e^- - h^+$) pairs are generated on CdS semiconductor. These photogenerated electrons will easily pass through the interface between the β -NiS film and CdS NFs, due to the intimate contact between them and the great conductivity of β -NiS film. They can further move to the surface of β -NiS film, where they will react with H₂O to form H₂. Simultaneously, the photogenerated h^+ on the surface of CdS that was not covered by the NiS film could react with the lactic acid molecules to form pyruvic acid [21]. In a word, the β -NiS film uniformly covered on the surface of the CdS NFs would enhance the transfer of photogenerated e^- , facilitating the separation of electron-hole ($e^- - h^+$) pairs and producing a large amount of active sites on the surface of the film, improving the rate of photocatalytic hydrogen evolution.

4. Conclusions

A novel NiS/CdS NFs HSNC was successfully synthesized via an electroless Ni plating method by using Cd(NO₃)₂·4H₂O as Cd-resource, CH₄N₂S as S-resource and Ni(CH₃COO)₂·4H₂O as Ni-resource with the presence of NaH₂PO₂·H₂O as the reducing agent. The optimum condition for the synthesis of NiS/CdS NFs HSNC on the basis of photocatalytic hydrogen evolution efficiency includes the orderly mixing of 1 mmol Cd(NO₃)₂·4H₂O, 3 mmol CH₄N₂S, 0.6 mmol Ni (CH₃COO)₂·4H₂O and 0.6 mmol NaH₂PO₂·H₂O in 50 mL of deionized water, and hydrothermal treatment at 180 °C for 4 h. Because of the strongly adhesive contact between the highly conductive β -NiS films and excellently visible-light-absorptive CdS NFs, which will produce a large amount of active sites on the surface of the composite, the as-synthesized NiS/CdS NFs HSNC presented much improved efficiency for photocatalytic hydrogen evolution in aqueous solution containing 20 vol.% lactic acid as the sacrificial agent. The highest rate for hydrogen production reached a recorded value of about

30.1 mmol h⁻¹ g⁻¹ at 25 °C among all the CdS-NiS composite catalysts, and the highest apparent quantum efficiency was approximately 43% at 420 nm. The growth and photocatalysis mechanisms for the NiS/CdS NFs HSNC were proposed.

Acknowledgments

The authors would like to thank the financial support for this work from the National Natural Science Foundation of China (grant nos. 11674035, 11274052 and 61274015).

References

- [1] Y. Moriya, T. Takata, K. Domen, Recent progress in the development of (oxy)nitride photocatalysts for water splitting under visible-light irradiation, *Coordin. Chem. Rev.* 257 (2013) 1957–1969.
- [2] Y. Xu, Y. Huang, B. Zhang, Rational design of semiconductor-based photocatalysts for advanced photocatalytic hydrogen production: the case of cadmium chalcogenides, *Inorg. Chem. Front.* 3 (2016) 591–615.
- [3] M.I. Jamesh, Recent progress on earth abundant hydrogen evolution reaction and oxygen evolution reaction bifunctional electrocatalyst for overall water splitting in alkaline media, *J. Power Sources* 333 (2016) 213–236.
- [4] N. Serpone, A.V. Emeline, V.K. Ryabchuk, V.N. Kuznetsov, Y.M. Artem'ev, S. Horikoshi, Why do hydrogen and oxygen yields from semiconductor-based photocatalyzed water splitting remain disappointingly low? Intrinsic and extrinsic factors impacting surface redox reactions, *ACS Energy Lett.* 1 (2016) 931–948.
- [5] A. Fujishima, K. Honda, Electrochemical photolysis of water at a semiconductor electrode, *Nature* 238 (1972) 37–358.
- [6] F.T. Li, J.R. Ran, M. Jaroniec, S.Z. Qiao, Solution combustion synthesis of metal oxide nanomaterials for energy storage and conversion, *Nanoscale* 7 (2015) 17590–17610.
- [7] S. Anantharaj, S.R. Ede, K. Sakthikumar, K. Karthick, S. Mishra, S. Kundu, Recent trends and perspectives in electrochemical water splitting with an emphasis on sulfide, selenide, and phosphide catalysts of Fe Co, and Ni: a review, *ACS Catal.* 6 (2016) 8069–8097.
- [8] N. Jiang, Q. Tang, M.L. Sheng, B. You, D.E. Jiang, Y.J. Sun, Nickel sulfides for electrocatalytic hydrogen evolution under alkaline conditions: a case study of crystalline NiS, NiS₂, and Ni₃S₂ nanoparticles, *Catal. Sci. Tech.* 6 (2016) 1077–1084.
- [9] F.K. Ma, Y.Z. Wu, Y.L. Shao, Y.Y. Zhong, J.X. Lv, X.P. Hao, 0D/2D nanocomposite visible light photocatalyst for highly stable and efficient hydrogen generation via recrystallization of CdS on MoS₂ nanosheets, *Nano Energy* 27 (2016) 466–474.
- [10] Q. Li, X. Li, S. Wageh, A.A. Al-Ghamdi, J.G. Yu, CdS/graphene nanocomposite photocatalysts, *Adv. Energy Mater.* 5 (2015) 1500010.
- [11] M.R. Gholipour, C.T. Dinh, F. Beland, T.O. Do, Nanocomposite heterojunctions as sunlight-driven photocatalysts for hydrogen production from water splitting, *Nanoscale* 7 (2015) 8187–8208.
- [12] J. Xu, X.J. Cao, Characterization and mechanism of MoS₂/CdS composite photocatalyst used for hydrogen production from water splitting under visible light, *Chem. Eng. J.* 260 (2015) 642–648.
- [13] Q.J. Xiang, F.Y. Cheng, D. Lang, Hierarchical layered WS₂/graphene-modified CdS nanorods for efficient photocatalytic hydrogen evolution, *ChemSusChem* 9 (2016) 996–1002.
- [14] J.H. Yang, D.G. Wang, H.X. Han, C. Li, Roles of cocatalysts in photocatalysis and photoelectrocatalysis, *Acc. Chem. Res.* 46 (2013) 1900–1909.
- [15] D.C. Jiang, Z.J. Sun, H.X. Jia, D.P. Lu, P.W. Du, A cocatalyst-free CdS nanorod/ZnS nanoparticle composite for high-performance visible-light-driven hydrogen production from water, *J. Mater. Chem. A* 4 (2016) 675–683.
- [16] Q.D. Yue, Y.Y. Wan, Z.J. Sun, X.J. Wu, Y.P. Yuan, P.W. Du, MoP is a novel, noble-metal-free cocatalyst for enhanced photocatalytic hydrogen production from water under visible light, *J. Mater. Chem. A* 3 (2015) 16941–16947.
- [17] Q. Li, B.D. Guo, J.G. Yu, J.R. Ran, B.H. Zhang, H.J. Yan, J.R. Gong, Highly efficient visible-light-driven photocatalytic hydrogen production of CdS-cluster-decorated graphene nanosheets, *J. Am. Chem. Soc.* 133 (2011) 10878–10884.
- [18] K. Chang, X. Hai, J.H. Ye, Transition metal disulfides as noble-metal-alternative cocatalysts for solar hydrogen production, *Adv. Energy Mater.* 6 (2016) 1502555.
- [19] Y.X. Li, H. Wang, S.Q. Peng, Tunable photodeposition of MoS₂ onto a composite of reduced graphene oxide and CdS for synergistic photocatalytic hydrogen generation, *J. Phys. Chem. C* 118 (2014) 19842–19848.
- [20] X. Zong, J.F. Han, G.J. Ma, H.J. Yan, G.P. Wu, C. Li, Photocatalytic H₂ evolution on CdS loaded with WS₂ as cocatalyst under visible light irradiation, *J. Phys. Chem. C* 115 (2011) 12202–12208.
- [21] W. Zhang, Y.B. Wang, Z. Wang, Z.Y. Zhong, R. Xu, Highly efficient and noble metal-free NiS/CdS photocatalysts for H₂ evolution from lactic acid sacrificial solution under visible light, *Chem. Commun.* 46 (2010) 7631–7633.
- [22] J. Zhang, S.Z. Qiao, L.F. Qi, J.G. Yu, Fabrication of NiS modified CdS nanorod p-n junction photocatalysts with enhanced visible-light photocatalytic H₂-production activity, *Phys. Chem. Chem. Phys.* 15 (2013) 12088–12094.
- [23] J.L. Meng, F.Y. Li, Y.M. Hu, L. Xu, Z.X. Sun, J. Liu, Facile preparation of NiS/CdS-t composite photocatalyst for hydrogen evolution from aqueous solution of sulphide/sulphite under visible light, *Mater. Res. Bull.* 48 (2013) 2111–2116.
- [24] J.L. Meng, Z.M. Yu, Y. Li, Y.D. Li, PdS-modified CdS/NiS composite as an efficient photocatalyst for H₂ evolution in visible light, *Catal. Today* 225 (2014) 136–141.
- [25] Z.X. Qin, Y.B. Chen, X.X. Wang, X. Guo, L.J. Guo, Intergrowth of cocatalysts with host photocatalysts for improved solar-to-hydrogen conversion, *ACS Appl. Mater. Inter.* 8 (2016) 1264–1272.
- [26] D.Y. Li, L.H. Feng, Z. Zheng, N. Li, Applications of sodium hypophosphite in electroless plating, *Electroplat. Pollut. Control* 34 (2014) 5–7.
- [27] J. Georgieva, S. Artyanov, Electroless deposition and some properties of Ni-Cu-P and Ni-Sn-P coatings, *J. Solid State Electrochem.* 11 (2007) 869–876.
- [28] K.K. Kar, D. Sathiyamoorthy, Influence of process parameters for coating of nickel-phosphorous on carbon fibers, *J. Mater. Proc. Tech.* 209 (2009) 3022–3029.
- [29] Q.H. Hu, X.T. Wang, H. Chen, Z.F. Wang, Synthesis of Ni/graphene sheets by an electroless Ni-plating method, *New Carbon Mater.* 27 (2012) 35–41.
- [30] R.H. Guo, S.X. Jiang, C.W.M. Yuen, M.C.F. Ng, J.W. Lan, Optimization of electroless nickel plating on polyester fabric, *Fiber. Polym.* 14 (2013) 459–464.
- [31] D.K. Lee, C.W. Ahn, H.J. Jeon, Web of carbon fibers coated with 3D snowflake-shaped Ni₃S₂/Ni produced by electroless Ni plating: a binder-free cathode electrode for lithium batteries, *Microelectron. Eng.* 166 (2016) 1–4.
- [32] Y. Zhang, Z.J. Peng, S.D. Guan, X.L. Fu, Data on the Synthesis Processes Optimization of Novel β-NiS Film Modified CdS Nanoflowers Heterostructure Nanocomposite for Extraordinarily Highly Efficient Photocatalysts for Hydrogen Evolution, (2017) Data in Brief, submitted.
- [33] S.C. Yan, Y. Shi, L.T. Sun, Z.D. Xiao, B. Sun, X. Xu, Controlled synthesis of NiS nanoparticle/CdS nanowire heterostructures via solution route and their optical properties, *Mater. Sci. Eng. B* 178 (2013) 109–116.
- [34] Q.Z. Wang, J.H. Lian, J.J. Li, R.F. Wang, H.H. Huang, B.T. Su, Z.Q. Lei, Highly efficient photocatalytic hydrogen production of flower-like cadmium sulfide decorated by histidine, *Sci. Rep.* 5 (2015) 13593.
- [35] H. Ashassi-Sorkhabi, S.H. Rafizadeh, Effect of coating time and heat treatment on structures and corrosion characteristics of electroless Ni-P alloy deposits, *Surf. Coat. Technol.* 176 (2004) 318–326.
- [36] D.C. Jiang, Z.J. Sun, H.X. Jia, D.P. Lu, P.W. Du, Cocatalyst-free CdS nanorods/ZnS nanoparticles composite for high-performance visible-light-driven hydrogen production from water, *J. Mater. Chem. A* 4 (2016) 675–683.
- [37] D.P. Kumar, S. Hong, D.A. Reddy, T.K. Kim, Ultrathin MoS₂ layers anchored exfoliated reduced graphene oxide nanosheet hybrid as a highly efficient cocatalyst for CdS nanorods towards enhanced photocatalytic hydrogen production, *Appl. Catal. B-Environ.* 212 (2017) 7–14.
- [38] C. Zhu, C.G. Liu, Y.J. Zhou, Y.J. Fu, S.J. Guo, H. Li, S.Q. Zhao, H. Huang, Y. Liu, Z.H. Kang, Carbon dots enhance the stability of CdS for visible-light-driven overall water splitting, *Appl. Catal. B-Environ.* 216 (2017) 114–121.
- [39] Z.J. Sun, H.F. Zheng, J.S. Li, P.W. Du, Extraordinarily efficient photocatalytic hydrogen evolution in water using semiconductor nanorods integrated with crystalline Ni₂P cocatalysts, *Energy Environ. Sci.* 8 (2015) 2668–2676.